Accuracy of Modal Stress Calculations by the Finite Element Method

HOWARD M. ADELMAN,* DONNELL S. CATHERINES,† AND WILLIAM C. WALTON JR.‡
NASA Langley Research Center, Langley Station, Hampton, Va.

A study was carried out to determine the preference of using a large number of elements having low-order displacement polynomials or a smaller number of elements having higher-order displacement polynomials. Calculations of the modal stresses in a clamped cylindrical shell were carried out using a finite element computer program. Three different displacement fields and five different element representations were used in the calculations. It was found that use of high-order displacement fields gave more accurate stresses with smaller sized matrices than did use of lower-order displacement fields. It is further noted that use of displacement fields having polynomials whose orders are less than three in the in-plane displacement components or less than five in the normal displacement component leads to unrealistic discontinuities in the stress distributions. It is, therefore, concluded that in finite element analysis of shells of revolution, polynomials representing the element displacement components should be at least third order in the in-plane displacement components and at least fifth order in the normal displacement component.

Introduction

IN static and dynamic analysis of shells of revolution, analysts have made extensive use of the finite element method. This method replaces the actual shell by an assemblage of elements whose displacement components are approximated (generally by polynomials). The behavior of the shell is then determined by solving a matrix equation. The accuracy of the solution is proportional to the number of elements used as well as the order of the polynomials which approximate the displacements within each element. Unfortunately, the size of the matrices involved and, consequently, the computer time are also proportional to the same parameters. Thus, the analyst is faced with a tradeoff to obtain the most accurate solution with the smallest sized matrices.

One way of increasing the efficiency has been to use element whose shapes resemble a portion of the shell. This has been the impetus for the development of several new elements such as the conical frustum element,[1,2] cylindrical element,[3,4] curved axisymmetric element,[5,6] and geometrically exact elements.[7,8]

Unfortunately, in most calculations with these elements, the simplest possible displacement field is used and a large number of elements are required to obtain accurate results.[1–6,9] This has required the solution of fairly large matrix equations (in excess of order 100). Thus some of the computational efficiency which motivated the development of these elements has been lost.

A possible way of recovering some of this efficiency is to use high-order polynomials in the assumed displacement field. There has been a certain amount of controversy about whether it is, in fact, more efficient to use higher-order polynomials or to simply increase the number of elements. References 2 and 9 suggest that simply using a large number of elements is better than using higher-order polynomials. However, some results in Fig. 6 of Ref. 2 suggested the opposite conclusion.

Presented as Paper 69-56 at the 7th Aerospace Sciences Meeting, New York, January 20–22, 1969; submitted January 30, 1969; revision received August 18, 1969.

* Aerospace Technologist. Member AIAA.
† Mathematician.
‡ Aerospace Technologist.

These results prompted an investigation reported in Ref. 8. The findings of this investigation were that in the calculation of natural frequencies of a cylindrical shell, a small number of elements with high-order displacement polynomials achieved better accuracy with smaller matrices than did a larger number of elements with lower-order polynomials.

This paper reports on a study similar to Ref. 8 but concentrating on modal stresses in a cylindrical shell. The study developed an algorithm based on the method of Ref. 10 to calculate exact modal stresses and natural frequencies of a cylinder clamped at each end. A mode was selected which exhibited a boundary layer in the stress because this constitutes a severe test of a finite element. Calculations were then carried out using the computer program of Ref. 7 using three different assumed displacement fields and several different numbers of elements. All the results from the computer program were compared to the exact solution. The conclusions reached in the study were consistent with Ref. 8, that is, a small number of elements with high-order displacement polynomials gave more accurate frequencies and stresses with smaller sized matrices than did a larger number of elements with low-order polynomials.

Essentials of the Finite Element Algorithm of Reference 7

Geometrically Exact Elements

Figure 1 shows the idealization of a typical shell of revolution by geometrically exact elements. The geometrically exact element is simply a slice of the shell being analyzed. No approximation of the shape of the shell is necessary. Functions of the meridional coordinate s describing the shape of the shell and describing the distributions of stiffness and mass are considered as input.

Element Stiffness and Mass Matrices

As shown in Fig. 2, u, v, and w represent displacement components in the meridional, circumferential, and normal directions, respectively. For a shell of revolution vibrating in a natural mode with circular frequency ω, the displacements

can be expressed as follows:

$$\begin{aligned} u(s,\theta,t) &= [u(s)\ \cos n\theta]e^{i\omega t} \\ v(s,\theta,t) &= [v(s)\ \sin n\theta]e^{i\omega t} \\ w(s,\theta,t) &= [w(s)\ \cos n\theta]e^{i\omega t} \end{aligned} \tag{1}$$

where 1) θ is the circumferential coordinate (see Fig. 2), 2) t is time, 3) $i = (-1)^{1/2}$, and 4) n takes on integral values.

Using the strain displacement relations of Novozhilov and the usual strain energy expression for shells (i.e., Ref. 7) along with Eq. (1), one is led to an expression for V, the amplitude of the strain energy of an element, having the form

$$V = \frac{1}{2}\int_{-\epsilon/2}^{+\epsilon/2} \{\xi\}^T[R]\{\xi\}dx \tag{2}$$

where 1) ϵ is the meridional length of the element (Fig. 1), 2) x is distance measured along the meridian of the element from the meridional center of the element, 3) $\{\xi\}$ is a column matrix given by

$$\{\xi\} = \{w(x),w'(x),w''(x),u(x),u'(x),v(x),v'(x)\} \tag{3}$$

where a prime denotes differentiation with respect to x, 4) T denotes the transpose of a matrix, and 5) $[R]$ is a 7×7 matrix, the elements of which are sums of rational functions of x arising out of the functions which describe the shape of the shell and the distribution of the elastic properties.

The assumed displacement field within the element is as follows:

$$w(x) = \sum_{j=0}^{j=N_w} a_j x^j,\ u(x) = \sum_{k=0}^{k=N_u} b_k x^k,\ v(x) = \sum_{l=0}^{l=N_v} c_l x^l \tag{4}$$

In the study to be discussed, three different expansions in polynomial terms, consistent with Eq. (4), are used to represent the displacements. The expansions are designated 1) third-order w, linear u and v, $(N_w,N_u,N_v) = (3, 1, 1)$, 2) third-order w, u, and v, $(N_w,N_u,N_v) = (3, 3, 3)$, and 3) fifth-order w, third-order u and v, $(N_w,N_u,N_v) = (5, 3, 3)$.

Substituting Eq. (4) into Eq. (3), substituting the resulting equation into Eq. (2), and then minimizing the strain energy expression in the usual way leads to a stiffness matrix for the element. The coordinates associated with this stiffness matrix are those coefficients among the a_j, b_k, and c_l included in the particular expansion of the displacements which is used. Thus, the dimensions of the stiffness matrix are 8×8, 12×12, or 14×14, depending on whether expansion (1), (2), or (3) is used.

After suitable transformations of coordinates, the element stiffness matrices can be assembled to form a stiffness matrix for the entire shell. This assembly is predicated on certain assumptions of continuity of the displacements and their derivatives at the points where one element joins another. These assumptions are summarized in Table 1.

Neglecting rotary inertia, the amplitude T of the kinetic energy of the system is given by the expression

$$T = \omega^2\bar{T} \tag{5}$$

where

$$\bar{T} = \frac{1}{2}\int_{-\epsilon/2}^{+\epsilon/2} \rho h(x)\{[w(x)]^2 + [u(x)]^2 + [v(x)]^2\}r(x)dx \tag{6}$$

in which 1) $\rho h(x)$ is the mass per unit area of the shell, and 2) $r(x)$ is the radius of the shell (see Fig. 2). Beginning with the substitution of Eq. (4) into Eq. (6), the derivation of the element mass matrices and the subsequent assembly of the mass matrix of the shell are completely analogous to the developments outlined for the stiffness matrices.

Table 1 Continuity of functions

Expansion	Functions required to be continuous across element junctures
(1)	w,w',u,v
(2)	w,w',u,u',v,v'
(3)	w,w',w'',u,u',v,v'

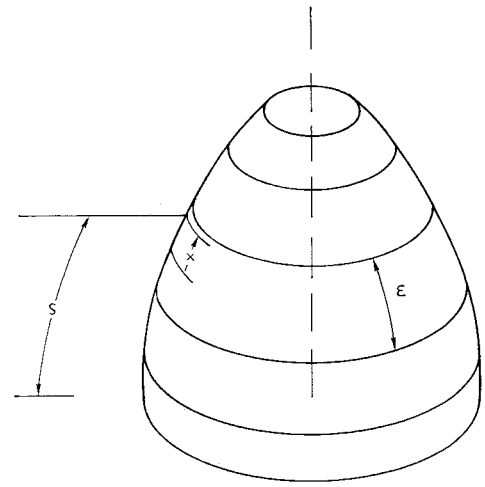

Fig. 1 Geometrically exact finite elements.

Exact Theory

The algorithm developed for computing the exact linear-theory modes for the shell was based on ideas originally advanced by Flugge and developed in a paper by Forsberg.[10] Novozhilov's shell theory was used in place of Flügge's, however.

Procedure of the Study

Description of the Cylinder

The dimensions and elastic constants of the cylinder which was treated are shown in Fig. 3. As physical units have no significant role in the study, the data describing the cylinder are given as dimensionless numbers. The cylinder is considered to be clamped at each end, by which it is meant that at each end

$$\begin{aligned} w &= 0 \\ w' &= 0 \\ u &= 0 \\ v &= 0 \end{aligned} \tag{7}$$

Definition of Variables

The mode selected for study was the mode of lowest frequency for $n = 3$. The reason for the choice was that calcu-

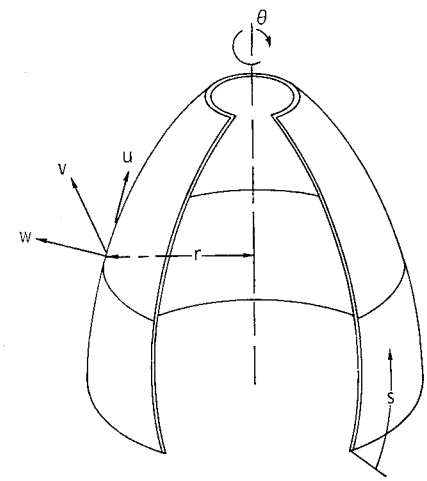

Fig. 2 Nomenclature.

Table 2 Summary of calculations

Idealization	Order of matrix equation, N	σ_a, max $\times 10^{-7}$	σ_a, center $\times 10^{-7}$	σ_c, max $\times 10^{-7}$	σ_c, center $\times 10^{-7}$	ω^2 $\times 10^{-7}$
Expansion (1)						
10 Equal 5a	36	5.16	3.40	1.55	0.829	5.744
10 Refined 5b	36	7.38	1.59	2.21	1.20	6.97
14 5c	52	9.15	1.59	2.74	1.20	6.92
28 5e	108	8.04	3.57	2.41	1.16	5.360
Exact solution	...	9.71	3.65	2.91	1.32	5.304
Expansion (2)						
10 Equal 5a	58	5.87	3.68	1.76	1.33	5.387
10 Refined 5b	58	6.70	3.75	2.01	1.34	5.320
14 5c	82	8.05	3.75	2.41	1.31	5.309
18 5d	106	9.12	3.75	2.73	1.34	5.306
Exact solution	...	9.71	3.65	2.91	1.32	5.304
Expansion (3)						
10 Equal 5a	69	7.50	3.66	2.25	1.32	5.315
10 Refined 5b	69	9.15	3.74	2.74	1.33	5.306
14 5c	97	9.63	3.74	2.89	1.33	5.306
Exact solution	...	9.71	3.65	2.91	1.32	5.304

lation by the exact solution showed that stress distributions in this mode are quite complicated near the clamped edges and the largest stresses in the mode occur in the region of the edge.

In all calculations of the mode, both by the exact method and by the finite element algorithm of Ref. 7, the mode was normalized so that

$$\int \rho h(w^2 + u^2 + v^2)dA = 1 \tag{8}$$

where ρh is the mass of the shell per unit area, w, u, and v are the modal displacements, and the integration indicated by $\int dA$ is taken over the surface of the shell.

The following six quantities (see Fig. 4) associated with the stress distribution were considered to be of interest and were computed as functions of x/L: 1) T_a, the axial stress resultant, 2) T_c, the circumferential stress resultant, 3) M_c, resultant moment about circumferential direction, 4) M_a, resultant moment about axial direction, 5) σ_a, outer fiber axial stress, 6) σ_c, outer fiber circumferential stress.

In order to be precise about the meanings of these six quantities, the following defining relations are introduced:

$$C = Eh/(1 - \mu^2) \tag{9}$$

$$D = Eh^3/[12(1 - \mu^2)] \tag{10}$$

$$e_a = u' \tag{11}$$

$$e_c = (1/r)(nv + w) \tag{12}$$

$$\kappa_a = -w'' \tag{13}$$

$$\kappa_c = (1/r^2)(n^2w + nv) \tag{14}$$

$$T_a = C(e_a + \mu e_c) \tag{15}$$

$$T_c = C(\mu e_a + e_c) \tag{16}$$

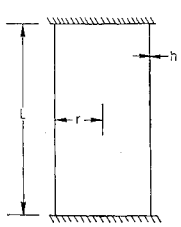

LENGTH	L	12
RADIUS	r	3
THICKNESS	h	.01
YOUNG'S MODULUS	E	3×10^7
POISSON'S RATIO	μ	.30
MASS DENSITY	ρ	7.33×10^{-4}

Fig. 3 Dimensions and material constants.

$$M_a = D(\mu\kappa_a + \kappa_c) \tag{17}$$

$$M_c = D(\kappa_a + \mu\kappa_c) \tag{18}$$

$$E_a = [e_a + (h/2)\kappa_a] \tag{19}$$

$$E_c = e_c + (h/2)\kappa_c \tag{20}$$

$$\sigma_a = [E/(1 - \mu^2)](E_a + \mu E_c) \tag{21}$$

$$\sigma_c = [E/(1 - \mu^2)](\mu E_a + E_c) \tag{22}$$

It will be recognized that e_a and e_c are the middle surface strains in the axial and circumferential directions, respectively, and that κ_a and κ_c are the middle surface changes in curvature, and E_a and E_c are the outer fiber stresses in the corresponding directions.

Procedure

As regards number and placement of elements to represent the shell, five trials were made. First, the shell was represented by 10 equal elements as shown in Fig. 5a. Maintaining this layout of elements, calculations were made of the six quantities of interest in connection with the stresses using each of the polynomial expansions (1), (2), and (3) in the elements. The results of these calculations are compared with the exact theory in Figs. 6–11. There was no mixing of expansions among the elements; that is, when expansion (1) was used in any one element it was used in all elements and similarly for expansions (2) and (3). The representation

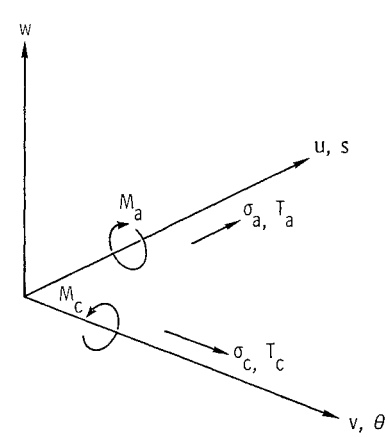

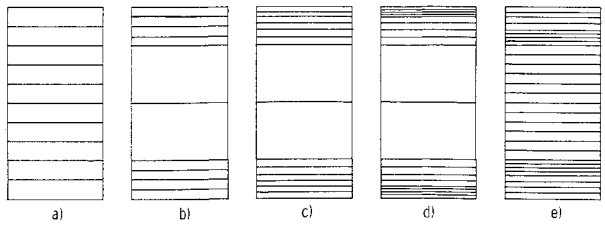

Fig. 5 Element layouts.

with 10 elements of equal length was used as a starting point because the work in Ref. 7, which was discussed in the introduction to the present paper and which led to the investigation reported in the present paper, was based on representations of the various shells with 10 elements of equal length. Based on consideration of the results of the calculations with the 10 elements of equal length, as explained in the next part of the paper, the layout of elements shown in Fig. 5b was tried. This layout consists of four relatively small elements of equal length adjacent to each end of the cylinder and two larger elements of equal length representing the middle portion of the cylinder. The small elements in the end regions are each of a length equal to $\frac{1}{20}$ the length of the cylinder, and the two larger elements representing the middle portion are each of a length equal to $\frac{9}{30}$ the length of the cylinder. The results of the layout shown in Fig. 5b, in turn, suggested the layout shown in Fig. 5c. The layout shown in Fig. 5c is obtained from the layout in Fig. 5b by dividing in half the two elements adjacent to each end. It was found that expansion (3) when applied to layout 5c gave essentially exact stresses. In order to compare the relative efficiency of high- or low-order polynomials, calculations were made using two additional refinements. These refinements are shown in Figs. 5d and 5e. Figure 5d was designed to be a further refinement of 5c such that when expansion (2) was applied to it, the number of degrees of freedom exceeded the number when expansion (3) was applied to 5c. Figure 5e was designed to be a refinement of 5c such that when expansion (1) was applied, the number of degrees of freedom exceeded that of any previous calculation. Refinement 5d was obtained from 5c by dividing in half the two elements adjacent to each edge. Refinement 5e was obtained from 5c as follows: the first four elements adjacent to each edge were left the same, the next two on each side were divided in half, finally the two large elements in the middle of the cylinder were divided into six equal elements. In the calculations for each of the layouts which have been discussed, the natural frequency of the mode was also generated. These calculations of the frequency are compared with the frequency computed by the exact theory in Table 2 in the next section of the paper.

Computing Effort

As a guide to estimating the relative computing effort and expense involved in the calculations, the following formula gives N the order of the eigenvalue problem which must be solved to yield the modes and frequencies of the clamped cylindrical shell.

$$N = \tfrac{1}{2}N_0(N_e + 1) - 8$$

where 1) N_e is the number of elements and 2) N_0 is the total number of polynomial terms representing the deflections in the element $N_0 = N_w + N_u + N_v + 3$.

The eigenvalue problem which is solved has symmetric stiffness and mass matrices. The mass matrix, which is positive definite, is not a diagonal matrix.

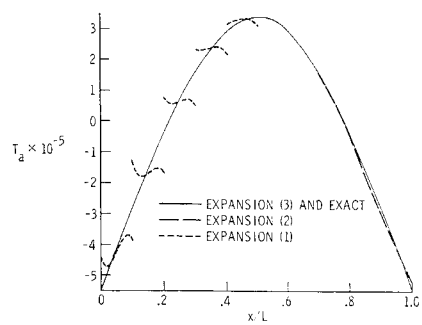

Fig. 6 Axial stress resultant T_a for 10 equal elements.

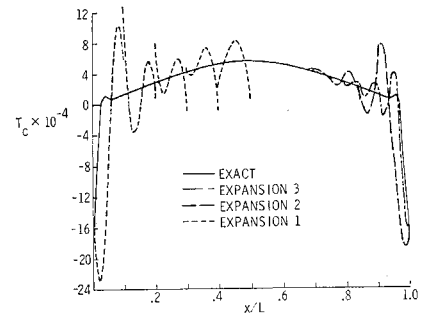

Fig. 7 Circumferential stress resultant T_c for 10 equal elements.

Results and Discussion

Stress Calculations with 10 Equal Elements

Axial stress resultant T_a (Fig. 6)

Exact theory gives a smooth curve for T_a with maximum value at the ends of the cylinder. Use of expansion (1) leads to a discontinuous curve for T_a the segments of which exhibit, generally, a roughly third-order variation with x/L. The trend of the level of stress in the segments follows the exact theory. Direct use of this approximate curve to predict stress would lead to large errors at many points along the shell, but the errors in the prediction of the maximum stress at the ends and the relatively large stress at the center would not be drastic. There would be an error in predicting the location of the maximum stress as the approximate theory achieves a maximum somewhat inboard of the ends of the shell. Expansion (2) gives a completely acceptable approximation of this stress resultant, and the curve resulting from use of expansion (3) is indistinguishable from the exact theory.

Circumferential stress resultant T_c (Fig. 7)

The exact curve for T_c varies smoothly over most of the interior of the shell but becomes complicated near the ends where there is a small hump and a precipitous gradient. The maximum value is reached at the ends. The curve resulting from the use of expansion (1) is discontinuous as in the previous figure, and the variations in the segments are even more complicated, giving a picture of the stress which,

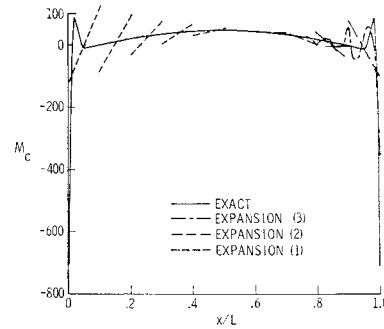

Fig. 8 Resultant moment about circumferential direction M_c for 10 equal elements.

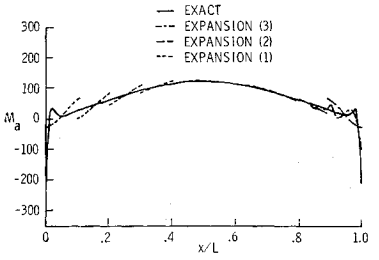

Fig. 9 Resultant moment about axial direction M_a for 10 equal elements.

although it has some coherence, would be tricky to use. Direct use of this curve to predict T_c would result in a substantial error in the prediction of the maximum value. Also, as in the previous figure, the location of the maximum is in error, as the maximum of the curve associated with expansion (1) is somewhat inboard of the end. Use of expansions (2) and (3) to compute T_c yields continuous curves. Both curves are coincident with the exact theory in the middle region of the shell, and both curves oscillate about the true curve as the ends are approached, resulting in distortions of the variation of T_c in the regions just inboard of the humps on the exact curve. However, use of expansion (2) gives a fair prediction of the maximum value of T_c and use of expansion (3) gives a very accurate prediction of the maximum value of T_c. The curve associated with expansion (2) peaks somewhat inboard of the ends, but the curve associated with expansion (3) peaks at the end, as does the true curve.

Resultant moment about the circumferential direction M_c (Fig. 8)

The exact curve for M_c is very smooth with gradual gradients over most of the shell but exhibits a very sharp-peaked hump and an extremely rapid rise in the regions of the ends. Use of expansions (1) and (2) results in discontinuous curves for M_c with the variations being linear in the segments. Use of expansion (3) gives a continuous curve for M_c which, however, has cusps. The curve associated with expansion (3) oscillates about the true curve as the ends are approached. The prediction of the maximum value of M_c is in gross error for all three expansions.

Resultant moment about the axial direction M_a (Fig. 9)

The nature of the exact curve for M_a and the degree of the approximations provided by use of expansions (1), (2), and (3) are substantially the same as for M_c.

Outer fiber axial stress σ_a (Fig. 10)

The exact curve for σ_a varies smoothly in the middle region of the shell in much the same manner as T_a. Near each end, however, there is a ledge and a steep gradient. Both expansions (1) and (2) give discontinuous curves for σ_a, but for expansion (2) the discontinuity is apparent only near the ends. In the middle region of the shell, use of expansion (1) reveals the trend of the stresses well and the results for expansions (2) and (3) are concident with the exact theory.

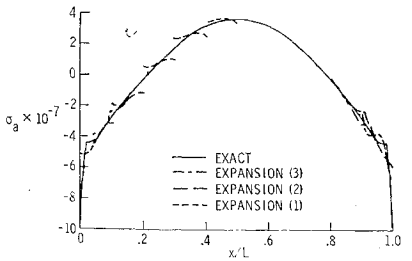

Fig. 10 Outer fiber axial stress σ_a for 10 equal elements.

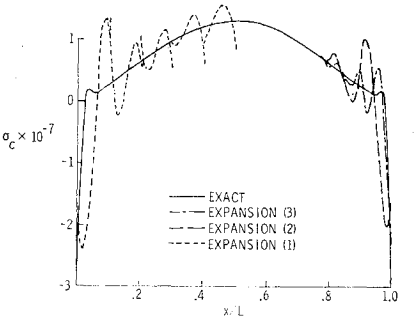

Fig. 11 Outer fiber circumferential stress σ_c for 10 equal elements.

As the regions of the steep gradients at the end are entered, however, none of the expansions represent the exact curve well. As would be expected, expansion (3) gives the best prediction for the maximum stress, but it is in error by more than 25%.

Outer fiber circumferential stress σ_c (Fig. 11)

The exact curve for σ_c varies smoothly in the middle regions much in the same manner as the exact curve for T_c. Near each end, however, there is a hump and a precipitous gradient. The curve generated for σ_c by use of expansion (1) is discontinuous with complicated variations in the segments. The curves generated by use of expansions (2) and (3) are continuous, but exhibit cusps and oscillate about the true curve in the end regions. As regards prediction of the maximum stress, the maximum value of the curve generated by expansion (1) is actually nearer the true value than the maximum values of expansions (2) and (3). However, this is regarded as the chance result of a rather wild variation of the curve for expansion (1) and is considered to be of no consequence. The prediction of maximum stress by use of expansion (3) is better than by use of expansion (2) but is in error by more than 20%.

Calculations with Refined Element Layouts (Figs. 12-17)

Based on the calculations with 10 equal elements, it was felt that errors are sufficiently exhibited by the outer fiber stresses. Therefore, in the remainder of the paper only these quantities are shown.

Using each of the three expansions with the layouts of Figs. 5b and 5c, calculations of outer fiber stresses were made and compared with the exact solution. The results from expansions (1) and (2) were still in substantial error and are not plotted. However, representative values of the stresses and also natural frequencies from expansions (1) and (2) are listed in the summary in Table 2. Using expansion (3) with layout 5b gives very good representations of the stress distribution with good predictions of the maximum stress. The approximate curves exhibit oscillations about the true curves in the immediate vicinity of humps and ledges but the excursions are not large. The results obtained by using expansion (3) with layout 5c are, for practical purposes, coincident with the exact curves. Using expansion (2) with layout

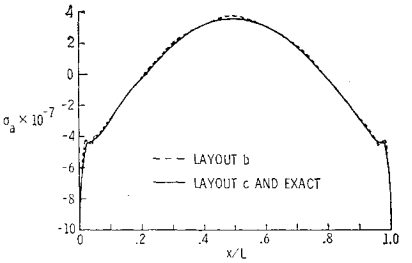

Fig. 12 Outer fiber axial stress σ_a for refined element layouts 5b and 5c and expansion (3).

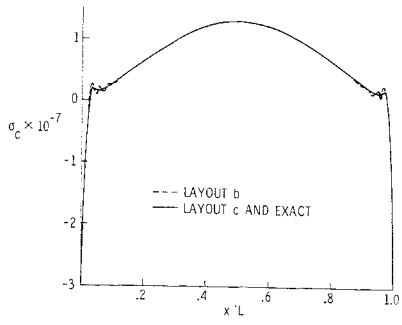

Fig. 13 Outer fiber circumferential stress σ_c for refined element layouts 5b and 5c and expansion (3).

5d, calculations of the stresses were made and compared with exact theory in Figs. 14 and 15. Although good over-all agreement was found, there is a 6% error in the maximum axial stress and 5.8% error in the maximum value of circumferential stress. Discontinuities in stress are not evident.

Using expansion (1) with layout 5e, the stresses were calculated and compared with exact theory in Figs. 16 and 17. The discontinuities in stress are quite evident. There is a 17.4% error in the maximum axial stress and 17.2% error in the maximum circumferential stress.

Summary of Calculations

Table 2 summarizes the computer runs that were carried out. For each calculation, the order of the matrices that resulted is listed along with the predicted values of outer fiber stress at the edge and at the midspan of the cylinder. In addition, the predicted natural frequency for each calculation is shown. The predictions of natural frequency are quite good for all cases except for the first three calculations made with expansion (1).

Inspection of this table clearly indicates the preference for using high-order polynomials in the displacement fields. For example, the calculation made with expansion (3) using idealization 5b gave better over-all stress and frequency results than did expansion (1) using idealization 5e despite the fact that the former calculation required matrices of order 69 and the latter required matrices of order 108.

Discussion

The results of this study indicate that in the calculation of natural frequencies and modal stresses of shells by the finite element method one should use displacement expansions at least as general as expansion (3). This conclusion is based on the following observations.

1) Use of expansion (3) in the element displacement field yields more accurate frequencies and modal stresses with smaller matrices than does use of the lower-order expansions.

2) Use of the lower-order displacement fields resulted in rather confusing stress predictions due primarily to the discontinuities in stress at element junctures. These discontinuities are a direct consequence of using polynomials which

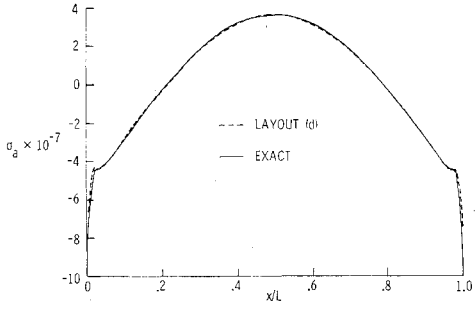

Fig. 14 Outer fiber axial stress σ_a for refined element layout 5d and expansion (2).

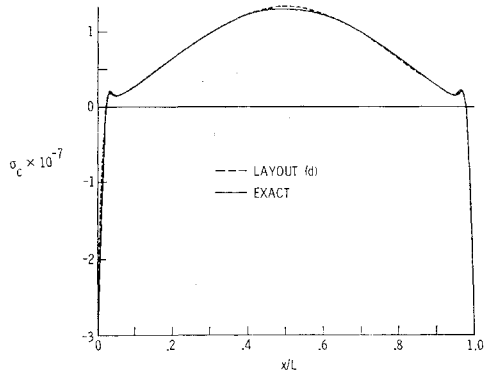

Fig. 15 Outer fiber circumferential stress σ_c for refined element layout 5d and expansion (2).

are of such a low order that they are discontinuous in derivatives which appear in the strain-displacement relations.

It will be recalled that there was a tendency of the approximate stress curves to oscillate about the true curves in regions where the flexibility of the representation was lacking, either due to elements which were too large or insufficient polynomial terms in the elements or both. It is suggested that the appearance of such oscillations in results calculated by the finite element method be taken as an indication of trouble and the representation should be refined in the region of the oscillations.

Finally, it is felt that results of this study indicate some practical significance in the question of whether all the complexities of the boundary-layer region, particularly the humps and ledges exhibited by the curves, represent physical fact or stem from some deficiency of the shell theory used. The authors do not here intend to suggest any particular deficiency or suggest a line of investigation with regard to this question. The only point raised is that the question has some importance relative to the effort required to predict the stresses in a shell with constraints.

Concluding Remarks

Using a finite element method developed in Ref. 7, a study has been conducted to arrive at a preferred representation of a shell for the purpose of predicting the complicated boundary-layer stress distributions which occur near clamped edges during vibration in a normal mode.

The finite element method was applied to compute the stresses in a mode exhibiting complicated boundary-layer stresses for a cylindrical shell clamped at each end. Several different combinations of number and placement of elements and number of polynomial terms in the displacement representations were used. The distributions of various kinds of stresses and stress resultants calculated by the finite element method were compared to calculations by exact theory. The following observations were made.

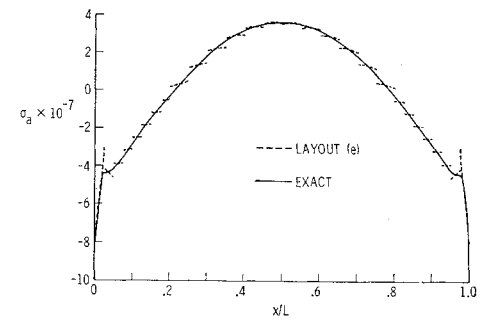

Fig. 16 Outer fiber axial stress σ_a for refined element layout 5e and expansion (1).

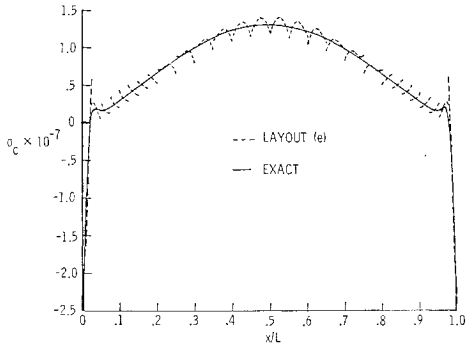

Fig. 17 Outer fiber circumferential stress σ_c for refined element layout 5e and expansion (1).

1) In vibration analysis of shells of revolution, one should use small elements near constraints and displacement expansions at least as general as fifth order in the normal displacement and third order in the in-plane displacements.

2) There is a tendency of approximate stress curves to oscillate about the true curves in regions where flexibility of the representation is lacking, either due to an insufficient number of elements or an insufficient number of polynomial terms in the assumed displacement field.

3) As regards the effort required to predict stresses in engineering uses of shells, it is important to determine if the complexities of boundary-layer stresses are physically realistic.

References

[1] Grafton, P. E. and Strome, D. R., "Analysis of Axisymmetrical Shells by the Direct Stiffness Method," *AIAA Journal*, Vol. 1, No. 10, Oct. 1963, pp. 2342–2347.

[2] Percy, J. H. et al., "Application of Matrix Displacement Method to Linear Elastic Analysis of Shells of Revolution," *AIAA Journal*, Vol. 3, No. 11, Nov. 1965, pp. 2138–2145.

[3] Bogner, F. K., Fox, R. L., and Schmit, L. A., "A Cylindrical Shell Finite Element," *AIAA Journal*, Vol. 5, No. 4, April 1967, pp. 745–750.

[4] Cantin, G. and Clough, R., "A Refined Curved Cylindrical Shell Finite Element," AIAA Paper 68-176, New York, Jan. 1968.

[5] Jones, R. E. and Strome, D. R., "Direct Stiffness Method Analysis of Shells of Revolution Utilizing Curved Elements," *AIAA Journal*, Vol. 4, No. 9, Sept. 1966, pp. 1519–1525.

[6] Stricklin, J. A., Navaratna, D. R., and Pian, T. H., "Improvements on the Analysis of Shells of Revolution by the Matrix Displacement Method," *AIAA Journal*, Vol. 4, No. 10, Nov. 1966, pp. 2069–2071.

[7] Adelman, H. M. et al., "A Method for Computation of Vibration Modes and Frequencies of Orthotropic Thin Shells of Revolution Having General Meridional Curvature," TN D-4972, Jan. 1969, NASA.

[8] Webster, J. J., "Free Vibrations of Shells of Revolution Using Ring Finite Elements," *International Journal of Mechanical Science*, Vol. 9, No. 8, Aug. 1967, p. 559.

[9] Klein, S., "Finite Element Solution for Axisymmetrical Shells," *Journal of the Engineering Mechanics Division, Proceedings of the American Society of Civil Engineers*, June 1965, p. 264.

[10] Forsberg, K., "Influence of Boundary Conditions on the Modal Characteristics of Thin Cylindrical Shells," *AIAA Journal*, Vol. 2, No. 12, Dec. 1964, pp. 2150–2157.